# On the role of Nav1.7 sodium channels in chronic pain: an experimental and

# computational study

Alberto Capurro<sup>1\*</sup>, Jack Thornton<sup>1</sup>, Bruno Cessac<sup>2</sup>, Lyle Armstrong<sup>1</sup>, Evelyne Sernagor<sup>1</sup>

- 1. Biosciences Institute, Faculty of Medical Sciences, Newcastle University, UK.
- 2. Université Côte d'Azur, Inria, Biovision team, France.

Chronic pain and Nav1.7 gating in human nociceptive neurons manuscript

\* Corresponding author

E-mail: alberto.capurro@newcastle.ac.uk

# 1 Abstract

2 Chronic pain is a global healthcare problem with a huge societal impact. Its management remains 3 generally unsatisfactory, with no single treatment clinically approved in most cases. In this study we 4 use an *in vitro* model of erythromelalgia consisting of dorsal root ganglion neurons derived from 5 human induced pluripotent stem cells obtained from a patient (carrying the mutation F1449V) and a 6 control subject. We combine neurophysiology and computational modelling to focus on the Nav1.7 7 voltage gated sodium channel, which acts as an amplifier of the receptor potential in nociceptive 8 neurons and plays a critical role in erythromelalgia due to gain of function mutations causing the 9 channel to open with smaller depolarisations.

Using extracellular recordings, we found that the scorpion toxin OD1 (a Nav1.7 channel opener) 10 11 increases dorsal root ganglion cell excitability in cultures obtained from the control donor, evidenced by an increase in spontaneous discharges, firing rate and spike amplitude. In addition, we confirmed 12 13 previous reports of voltage clamp experiments concerning an increase in spontaneous discharge in 14 the patient cell cultures and the analgesic effects of the Nav1.7 blocker PF-05089771. Our findings 15 are explained with a conductance-based model of the dorsal root ganglion neuron, exploring its 16 behaviour for different values of half activation voltage and inactivation removal rate of the Nav1.7 17 current. Erythromelalgia was simulated through a decrease of the Nav1.7 half activation voltage, 18 turning previously subthreshold stimuli to pain-inducing, and successfully counteracted with the 19 channel blocker. The painful effects of OD1 were simulated through a quicker removal of Nav1.7 20 inactivation that reproduced the effects of the toxin not only on the spike frequency but also on its 21 amplitude.

## 22 New & Noteworthy

We investigate Nav1.7 channel gating mechanisms in human iPSC-derived dorsal root ganglion cell cultures using multielectrode array recordings. The scorpion toxin OD1 increases firing frequency and spike amplitudes whilst the analgesic PF-05089771 decreases or even abolishes spontaneous activity. The antagonistic effect of these compounds is explained with a computational model to

27 reach deeper understanding of changes in channel kinetics in erythromelalgia, a chronic pain

28 disorder.

## 29 Introduction

Chronic pain is a global healthcare problem, particularly affecting elderly people, women and 30 31 persons with lower socio-economic status (Van Hecke et al., 2013). It is one of the most common 32 reasons for physician consultation in developed countries, interfering with quality of life and causing 33 large socio-economic impacts that include significant loss of working hours and the need of clinical care. Current therapies have limitations in their effectiveness and side effects, creating an urgent 34 need to develop more precise and effective treatments for pain management (Khouzam, 2000). In 35 36 this study we focus on the voltage dependent properties of the sodium channel Nav1.7 that is 37 implicated in inherited erythromelalgia, a vascular peripheral pathology causing attacks of severe 38 chronic pain (McDonnell et al., 2016).

39 Pain evoked spiking activity starts in peripheral terminals of dorsal root ganglion (DRG) neurons. The 40 central extensions of these neurons form the A $\delta$  and C fibres which establish glutamatergic synapses 41 onto second order neurons within the spinal cord. They can be stimulated by mechanical, thermal or 42 chemical stimuli as well as by inflammatory mediators. Distributed throughout the body (skin, 43 viscera, muscles, joints, meninges), they carry noxious sensory information into the central nervous 44 system (Serpell, 2006). The recent discovery of nociceptive Schwann cells has changed the notion of 45 bare nerve terminals being the starting point of pain sensation, and introduced the concept of a glio-46 neural end organ in the skin that transmits nociceptive information to the nerve, resembling the 47 specialized receptor cells found in other sensory systems (Abdo et al., 2019).

DRG neurons express several types of voltage gated sodium channels with different properties (Lera Ruiz and Kraus, 2015). The opening of Nav1.7 channels requires smaller depolarisations than other types of sodium channels, being more easily activated by the graded generator potentials. For this reason it is considered to be a threshold channel that acts as an amplifier of the receptor potential, increasing the probability of triggering a spike via the activation of other, higher threshold sodium channels such as Nav1.8. This amplification property makes Nav1.7 a major contributor to pain signalling in humans (Dib-Hajj et al., 2013).

Erythromelalgia is caused by gain 2 of 2 function mutations of the gene SCN9A, which encodes for the Nav1.7 channels pain (McDonnell et al., 2016). Different types of mutations have in common the need for less depolarization to open the channel than in the wild type, resulting in a decrease of the rheobase (i.e., minimal amplitude of an infinite depolarizing current to evoke a spike) (Cao et al., 2016). DRG neurons fire spontaneously in erythromelelgia patients, although normally these cells are silent unless receiving strong peripheral pain stimulus.

61 In this study, we have used extracellular recordings of spontaneous activity in DRG neuron cultures 62 derived from human induced pluripotent stem cells (hiPSCs) obtained from an erythromelalgia 63 patient and a control subject to study the voltage dependent gating properties of Nav1.7 channels. 64 To start, the effects on the neuronal firing of two different pharmacological compounds -a pain 65 eliciting scorpion toxin (OD1, Motin et al., 2016) and an analgesic drug (PF-05089771, Cao et al., 66 2016)- were assessed in these cultures using multi electrode array (MEA) recordings. We then 67 present a simple conductance-based computational model of the DRG neuron to explain our findings 68 in terms of the Nav1.7 gating process, focusing on the channel activation (opening) and repriming 69 (i.e., recovery from inactivation).

70 Materials and Methods

# 71 Cells and MEA recordings

For this study we used hiPSCs from a control subject (cell line AD3) and an erythromelalgia patient (cell line RCi002-A, carrying the mutation F1449V) made available at the European Bank for induced pluripotent stem cells (EBiSC). The cells were differentiated into sensory neurons using a small 75 molecule based protocol described previously (Cao et al., 2016, and references therein). Once they 76 reached the stage of DRG neurons, the cells were re-plated in 24 wells MEA plates (MEA700, 77 Multichannel Systems, Reutlingen, Germany) where the spontaneous activity was recorded after 10 78 weeks of maturation. Each well contains 12 circular electrodes (100 µm diameter, 700 µm electrode 79 pitch), making a total of 288 electrodes per plate. The large distance between electrodes makes it very unlikely that the activity originating from an individual neuron will be detected by adjacent 80 electrodes. On the other hand, due to the relatively large cell density in these cultures, which 81 82 organize in structures called neural rosettes (e.g., Wilson and Stice, 2006), it is quite likely that one for details 83 electrode can detect the activity of more than one neuron (up to four in our data sets, although 84 most channels had only one or two).

85 We compared the spontaneous activity of DRG neurons obtained from a control subject (plated in 86 18 wells, making a total of 216 electrodes in MEA 1) with an erythromelalgia patient (plated in 24 87 wells, making a total of 288 electrodes in MEA 2). In addition we used a third MEA plated with 88 diseased cells stimulated with higher concentration of potassium (from 4.16 mM in the growing 89 medium to 6 mM) to enhance spontaneous activity (plated in 24 wells, making a total of 288 90 electrodes in MEA 3). This allowed us to find more active neurons following the addition of PF-91 05089771 to make paired comparisons before and after this treatment that tends to suppress the 92 firing in many channels. Each well constitutes an independent cell culture.

The cultures were treated with OD1 (100 nM) in the control subject (MEA 1) and with PF-05089771 (100 nM) in the patient (MEAs 2 and 3). The activity was recorded for 5 minutes immediately before the application of each substance and compared with a recording of the same duration performed 5 minutes after the onset of drug exposure. Wells contained 200 µl of growing medium and 5 µl drops were added to apply the treatments. The experimental doses were selected to be in a near saturation range to ensure a strong effect, based on dose response curves published previously (Cao

99 et al., 2016 for PF-05089771; Motin et al., 2016 for OD1). Both compounds were purchased from

100 Tocris (Bio-Techne, Abingdon, UK).

# 101 Spike sorting and pairing of units

Recordings were performed with the Multiwell-MEA-System and the software Multi Channel
Experimenter (Multi Channel Systems, Reutlingen, Germany). Each channel was band-pass filtered
(100 to 3500 Hz) and acquired with a sampling rate of 20 kHz.

105 The raw voltage traces were first plotted and inspected using a zoom tool to discard artefacts and 106 confirm the existence of spikes. The voltage time series were then fed into the Matlab toolbox 107 Waveclus (Quian Quiroga et al., 2004) to perform spike sorting in all active channels. In the toolbox, the continuous data were filtered again with a non-causal band pass filter between 300 and 3000 Hz 108 109 and the firing times were detected with an amplitude threshold. We used a dual threshold (i.e., 110 picking deflections in both up and down directions) set to 5 median absolute deviations of the 111 filtered voltage signal with a refractory period of 2 ms to avoid double annotations due to fast 112 voltage oscillations in the vicinity of the threshold. Spikes were aligned to their maximum, after 113 interpolating the waveforms to locate the peak time more accurately. The toolbox uses a wavelet 114 based method for feature extraction, and the grouping of spikes into clusters is done with super-115 paramagnetic clustering (Blatt et al., 1996), a stochastic algorithm that does not assume any 116 particular distribution of the data. In few cases the dual threshold created mistakes in the detection, 117 so we decided to use a single threshold, kept for the units that corresponded to the same neuron 118 before and after a given treatment. We consider this spike sorting strategy as supervised, always 119 following the criterion of the biologist as ground true. The firing times and voltage cut outs of all 120 units were stored to document the parameters and quality of the spike sorting in each channel.

121 Units that were active both before and after each pharmacological treatment were identified. The 122 only set-in-stone criterion for deciding if they are the same cell is the coordinates of the current 123 sources, using high density MEAs (Hilgen et al., 2017). As our data were recorded with low density 124 MEAs, we cannot provide this level of certainty, but assumed that they corresponded to the same 125 neuron if the wave shape remained similar across recordings performed within few minutes of each 126 other. Possible ambiguities were minimized by the fact that most channels yielded only one or two 127 active neurons. These pairs were used to investigate the changes in spike frequency and amplitude 128 caused by the pharmacological treatments (Figs 1 and 2). If we were reasonably convinced that a 129 given unit corresponded to the same neuron before and after treatment, we designated the two 130 recordings as a pair. In the case of the control cultures, few neurons had spontaneous discharges 131 and most cells started to fire only after the OD1 treatment. Conversely, in the case of the patient cultures, several neurons were active before, but few remained active after the application of PF-132 133 05089771. In that case, we made an additional recording after increasing the spontaneous activity 134 with potassium, as mentioned above. This manipulation allowed to get more active neurons in control conditions, and then more neurons remained active after the treatment to configure pairs, 135 although we did not pool the data recorded with and without higher potassium concentration. 136

For statistical comparisons between two conditions we used the Wilcoxon signed rank test (for paired values) or the Mann–Whitney U test (for unpaired values). We also used cross correlation histograms of the spike times recorded from the same channel to assess whether neurons tend to fire at fixed delay from another.

### 141 Numerical simulations

We performed numerical simulations of the membrane potential and sodium channels gate parameters of a single DRG neuron using the software NEURON (<u>www.neuron.yale.edu</u>), e.g., Choi et al., 2011). The integration method was the IDA algorithm (e.g., Carnevale, 2007) with a fixed time step of 0.025 ms (i.e., 40 time steps per ms). Our purpose is to explain the changes in frequency and amplitude induced by the drug treatments covered in the previous section. In this context we adopted a parsimonious approach to keep the model as simple as possible, using Hodgkin and Huxley (HH) type of Na<sup>+</sup> and K<sup>+</sup> currents (Ermentrout and Terman, 2010) with parameters (Table 1) adapted to be plausible for mammal cells (Krouchev et al., 2015) plus a single Nav1.7 type current

added using the Channel Builder GUI (McDougal et al., 2017).

151 The two different types of sodium channels that we included differed only in their parameters (Table 152 1), the form of the equations was the same (S1 Appendix). The first, with larger conductance (0.3  $S/cm^{2}$ ) and a more depolarized value of half activation voltage (d = -40 mV) resembles a HH type 153 154 high threshold Na<sup>+</sup> channel (like Nav1.8 in mammals). The second type of Na<sup>+</sup> channel, with a half activation voltage shifted in the hyperpolarizing direction (d = -55 to -60 mV) and a smaller value of 155 156 maximum conductance (0.1 S/cm<sup>2</sup>), represented a Nav1.7. It had faster opening/closing and 157 activating/inactivating rates and a more depolarized value of half inactivation voltage removal than the HH type channel (Table 1). These changes allowed to create a rapidly activating but slowly 158 repriming (slow recovery from inactivation) current, resembling Nav1.7. To simulate erythromelalgia 159 160 we varied the half activation voltage of Nav1.7 from -55 to -60 mV. To simulate PF-05089771 effect, we varied the maximum conductance of Nav1.7 from 0.1 to 0.07 S/cm<sup>2</sup> (Figs 3 and 4) and to simulate 161 162 OD1 effects (Figs 5, 6 and 7) we increased 10 times the parameter  $A_b$  that multiplies the inactivation 163 removal rate  $a_h$ . Model parameters are provided in Table 1, the equations that are most relevant for 164 our results appear in section Results and all model equations are listed in S1 Appendix.

Step depolarisations of 0.04 nA lasting 60 ms were used to evaluate the effect of the half activation voltage  $(d_h)$  and the inactivation removal rate  $(a_h)$  on the firing frequency of the spike (Figs 3 and 5). To estimate more reliably the spike frequency and amplitude by averaging over many spikes we used depolarization steps lasting 5 s (Figs 4 and 6).

169 In order to assess for bifurcations in the dynamical system, we performed simulations of the 170 maximum and minimum values of the voltage oscillation as a function of the amount of external 171 current injected (i.e., a one dimensional bifurcation diagram, e.g., Fig 3 in Doi et al., 2001, for  $d_m = -$ 172 58 mV and  $g_{max} = 0.1$  S/cm<sup>2</sup>.

- 173 All figures of the article were created with Matlab (R2018b, The MathWorks, Inc., Natick,
- 174 Massachusetts, United States) and finalized with Adobe illustrator (Adobe Inc.).

# 175 **Results**

### 176 Experimental recordings

We compared the spontaneous activity of DRG neurons obtained from a control subject (cell line 177 AD3, n = 18 cultures) with an erythromelalgia patient (cell line RCi002-A, n = 24 cultures). The 178 179 percentage of electrodes showing activity was 1.85 % in the control and 5.9 % in the disease 180 cultures. After spike sorting we found 30 spontaneously active units in the patient and only 7 in the 181 control. The firing frequency and amplitude of these units were not significantly larger in the disease 182 cultures, implying that although much more units are active, they do not necessarily fire faster or 183 have spikes of larger amplitude. It is worth mentioning that the fastest neurons and the tallest spikes 184 were found in the disease cultures, but the distributions were not significantly different because 185 slow units with small amplitude were present in both groups. The larger number of spontaneously 186 active neurons found in the disease cultures is consistent with the results of a previous study (Cao et 187 al., 2016).

The cultures from the control subject were treated with OD1 (100 nM), resulting in the percentage of active channels increasing from 1.85 to 6.02 % and a concomitant increase in the number of active units, from 7 to 24. An example of the voltage data before and after treatment is presented in Fig 1-A, note the large increase in spontaneous activity. The same picture was observed in an erythromelalgia culture conducted just as a verification (not shown).

Pairing all the units that were active before and after OD1 application in the control cells (n = 7), we found that both the spike frequency and amplitude increased significantly (Fig 1-B). Although the increase in amplitude was not dramatic (20 % in average), it was consistently found in every pair of units. The extent of the increase in firing frequency was more pronounced (70 %). The unpaired units 197 that were initially silent and started to fire after the OD1 were not significantly different in rate and

amplitude from those already active before the treatment.

The cells from the patient were treated with PF05089771 (100 nM). The percentage of channels with spiking activity fell from 5.9 to 2.08 %. An example of the raw voltage trace before and after treatment is presented in Fig 2-A, note that the spiking activity is decreased, although this particular recording was done in the presence of higher K<sup>+</sup> concentration.

Pairing the units that were active before and after the treatment (n=6), we found that the spike frequency decreased significantly but the amplitude did not change (Fig 2-B). This result was confirmed with a larger number of paired units (n=16) in a MEA plate previously exposed to high potassium concentration (Fig 2-C). In both cases the unpaired units that stopped firing as a result of the PF05089771 application were not significantly different in rate and amplitude to the ones that remained active after treatment.

209 In order to assess for possible functional connectivity, we calculated cross correlation histograms 210 between the firing times of the neurons that were recorded from the same electrode. No histogram 211 peaks at fixed latency were found, which is compatible with the established notion that DRG 212 neurons do not form synaptic contacts between them.

### 213 Numerical simulations

In this subsection we present the results obtained with the computational model of the single DRG
neuron explained in section Methods, including the equations directly related with the quantities
plotted in the figures. The equations of all currents are provided in S1 Appendix.

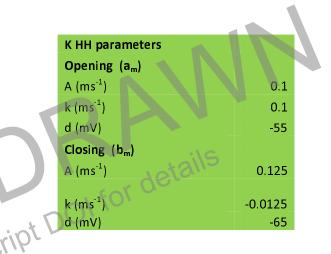
Our DRG neuron was simulated as a cylindrical soma of 30  $\mu$ m diameter and height. The ionic conductances are based on a HH model with mammalian-plausible parameters plus an additional Na<sup>+</sup> current with the features of a Nav1.7 (Table 1). The disease and health conditions were simulated through changes in the Nav1.7 half-activation voltage parameter ( $d_m$  in equation 1). In

- erythromelalgia patients, this parameter is shifted up to 15 mV in hyperpolarizing direction (Cao et
- al., 2016), causing a decrease in the level of depolarization needed to activate the Nav1.7 current.

223

224

General parameter set		
L (μm)	30	
d (µm)	30	
cm (μF/cm²)	1	
gNa_hh (S/cm²)	0.3	
gNav1.7_hh (S/cm²)	0.1	
gK_hh (S/cm²)	0.15	
	3.00E-	
gL_hh (S/cm <sup>2</sup> )	05	
eL_hh (mV)	-65	
eK (mV)	-90	- 1
eNa (mV)	60	<b>)</b>
Initial V (mV)	-75	
dt (ms)	0.025	
Temp (Celsius)	37	



Na HH parameters	
Opening (a <sub>m</sub> )	
A (ms <sup>-1</sup> )	1
k (ms <sup>-1</sup> )	0.1
d (mV)	-40
Closing (b <sub>m</sub> )	
A (ms <sup>-1</sup> )	4
k(ms <sup>-1</sup> )	-0.055
d (mV)	-65
Inactivation removal (a <sub>h</sub> )	
A (ms <sup>-1</sup> )	0.07
k (ms <sup>-1</sup> )	-0.05
d (mV)	-65
Inactivation establishment (b <sub>h</sub> )	
A (ms <sup>-1</sup> )	1
k (ms <sup>-1</sup> )	-0.1
d (mV_	-35

Nav1.7 parameters		
Opening (a <sub>m</sub> )		
A (ms <sup>-1</sup> )	13.78	
k (ms⁻¹)	0.1	
d (mV)	-58	
Closing (b <sub>m</sub> )		
A (ms <sup>-1</sup> )	55.11	
k (ms⁻¹)	-0.055	
d (mV)	-65	
Inactivation removal (a <sub>h</sub> )		
A (ms <sup>-1</sup> )	0.92	
k (ms⁻¹)	-0.05	
d (mV)	-40	
Inactivation establishment (b <sub>h</sub> )		
A (ms <sup>-1</sup> )	8.76	
k (ms <sup>-1</sup> )	-0.1	
d (mV)	-35	

225

226 Table 1. Default parameter values used for the simulations. Particular cases are indicated in the

- 227 corresponding figures.
- 228 The rate of Nav1.7 channel opening  $a_m$  is given by

229 
$$a_m = \frac{A_m \left(k_m \left(\nu - d_m\right)\right)}{1 - e^{-k_m \left(\nu - d_m\right)}}$$
(1)

- where v is the membrane potential,  $d_m$  is the half-activation voltage, and  $k_m$  and  $A_m$  are constants 230
- 231 (Table 1). The opening and closing dynamics of the current is given by the differential equation

$$232 \qquad \frac{am}{dt} = a_m(1-m) - b_m m$$

- rate ar 233 where m is the opened state of the channel, 1-m the closed state and  $b_m$  the closing rate.
- 234 The conductance is a cubic function of *m*,

235 
$$g_{Nav1.7} = g_{max} m^3 h$$

where h is the inactivation process and  $g_{max}$  the maximum conductance. 236

(2)

237 In Fig 3 we show the effects of varying  $d_m$  (Equation 1) in the model neuron by displaying the 238 response to a depolarizing current step of 0.04 nA lasting 60 ms. This level of current is slightly above the firing threshold at  $d_m$  = -58 mV and  $g_{max}$  = 0.1 S/cm<sup>2</sup>, which is 0.037 nA. At this threshold the one 239 240 dimensional bifurcation diagram (not shown) presents a discontinuity that corresponds to a Hopf 241 bifurcation (see section Discussion). The upper blue trace represents a normal subject ( $d_m$  = -55 mV) 242 where the stimulus does no elicit pain (i.e., no spiking). The pink traces of the middle row represent 243 mild erythromelalgia ( $d_m$  = -58 mV) where the same stimulus is painful (spiking in the left panel) and 244 can be successfully treated by blocking 20% of the Nav1.7 channels, i.e., decreasing the maximum conductance ( $g_{max}$  in Equation 3) from 0.1 to 0.08 S/cm<sup>2</sup> (no spiking in the right panel). In the red 245 246 traces of the lower row we simulate severe erythromelalgia ( $d_m = -60 \text{ mV}$ ), showing faster spiking 247 rate (left) and spontaneous spikes occurring before and after the stimulus. In this case, blocking 20% 248 of the Nav1.7 channels decreases the firing but is not able to stop it (middle panel). The pain eliciting

firing can be stopped by blocking a larger percentage of Nav1.7 channels (30% with  $g_{max} = 0.07$ S/cm<sup>2</sup>, right panel).

251 In Fig 4 we provide a qualitative frame to understand the situations described in the previous figure. 252 Using a heat map, the spike rate of the neuron model (stimulated with 0.04 nA depolarizing current) 253 is represented with a color bar for different values of maximum conductance  $g_{max}$  (Equation 3, 254 abscissas) and half activation voltage parameter  $d_m$  (Equation 1, ordinates) of the Nav1.7 current. 255 The white circles with numbers on the heat map indicate the coordinates  $(g_{max}$  and  $d_m)$  used for the 256 simulations depicted in Fig 3. The numbers inside the circles of Fig 4 correspond to the numbers in 257 the panels of Fig 3. Erythromelalgia mutations cause pain through a downward shift toward the red 258 values of the heat map (e.g., trajectories 1 to 2 and 2 to 4). Conversely, the treatment with Nav1.7 259 blockers (e.g., PF05089771) alleviates pain through a shift to the right, towards the blue values (e.g., trajectories 2 to 3 and 4 to 5 and 6). 260

In a second series of simulations we explored the inactivation properties of Nav1.7 channels (parameter sets displayed in Table 1). The scorpion toxin OD1 has been reported to increase the rate at which Nav1.7 inactivation is removed after being established (Motin et al., 2016). In order to emulate this effect in the model, we increased 10 times the removal rate of Nav1.7 inactivation ( $a_h$ in Equation 4).

266 The inactivation removal rate is given by

$$267 a_h = A_h e^{k_h(\nu - d_h)} (4)$$

where v is the membrane potential,  $k_h$  and  $A_h$  are constants (Table 1) and  $d_h$  is the half-inactivation

removal parameter. The inactivation process dynamic is given by the temporal derivative of h

270 
$$\frac{dh}{dt} = a_h(1-h) - b_h h$$
 (5)

where 1-h is the inactivated state and h is the non-inactivated state that allows ionic conduction.

272 To increase  $a_b$  we increased the multiplicative constant  $A_b$  by 10 times (Equation 4). This change 273 caused the model neuron to fire in response to a depolarizing pulse of 0.04 nA that was not effective 274 before (upper panels in Fig 5) and elicited a faster firing rate if the neuron was already active in the 275 control condition (lower panels in Fig 5).

276 The faster removal of Nav1.7 inactivation ( $A_b$  varied from 0.92 to 9.2) also increased the model spike 277 amplitude to a moderate amount in the simulation after OD1 (red plot in Fig 6), as observed in the 278 extracellular recordings (Fig 1-B). In Fig 7-A, we show plots of m (thin full lines) and h (dashed lines) 279 during a spike, in a simulation before (blue plots of left panel) and after OD1 (red plots of right 280 panel). Both panels display the Nav1.7 current with full thick lines. Note that in the simulation after OD1, Nav1.7 has larger amplitude, and the values of h are higher, with a faster return to 1 after the 281 282 negative peak. These large changes of h were not observed in the HH type high threshold sodium 283 current, although the current amplitude was slightly increased (Fig 7-B). see ma

#### 284 Discussion

285 In this study, we performed to our knowledge the first test of the scorpion toxin OD1 in hiPSC-286 derived DRG neurons. This toxin enhances the recovery from fast inactivation of the threshold 287 current Nav1.7 (Motin et al., 2016). Our extracellular recordings also confirmed previous findings of 288 Cao et al. (2016) with patch clamp regarding the increased spontaneous firing of erythromelalgia 289 DRG cells and the analgesic effects of PF-05089771. This drug was shown to be clinically effective to 290 control heat induced pain attacks by stabilizing the voltage sensor domain of the Nav1.7 channel in a 291 non-conducting conformation. The effects of both compounds were explained using a conductance-292 based computational model, comparable with Choi et al. (2011) but simpler and particularly 293 focalized on the issue of pain signalling. In this section we first discuss our main findings and 294 emphasize the usefulness of extracellular recordings to observe changes in ionic currents. To close 295 the discussion, we provide a short remark about the importance of the interaction between 296 different sodium currents in erythromelalgia.

### 297 Effects of erythromelalgia, PF-05089771 and OD1

298 Cao et al. (2016) performed voltage clamp experiments in whole-cell configuration in DRG cells 299 derived from erythromelalgia patients and control subjects. Despite the heterogeneity of the 300 samples, they found a significantly higher proportion of spontaneously firing cells in patients 301 compared to those from control donors. Moreover, the patient's cells showed a lower rheobase and 302 reached higher firing rates in response to stimulation with current steps of increasing amplitudes. 303 These findings point to the existence of elevated excitability in erythromelalgia cells, a fact that we 304 confirmed in the present study by showing higher prevalence of spontaneous activity in extracellular details 305 MEA recordings (section Results).

Spontaneous firing in our cultures is due only to intrinsic cell excitability, as there are no reports about the formation of synapses between DRG cells *in vitro*. Accordingly, we did not find evidence of functional connections in cross correlation histograms between neuronal firing times. Furthermore, in dissociated cell cultures the development of a synaptic network is usually accompanied by the emergence of population bursts (Maeda et al., 1995) which we did not observe here. DRG glia cells are not present in the cultures, so their reported contribution to abnormal neuronal activity in *in vitro* studies done on intact DRG (Belzer and Hanani, 2019) can also be ruled out.

Regarding the effects of Nav1.7 channel blockers, Cao et al. (2016) reported a dose dependent reduction in spontaneous firing and an increase in the action potential rheobase. We were able to reproduce the first finding on spontaneous firing with PF-05089771 (Fig 2), supporting the fact that the excitability of the cells plummets after the treatment, in accordance with the reported clinical efficacy of the drug (Cao et al., 2016). We did not, however, observe significant changes in spike amplitudes before and after drug treatment.

The effect of OD1 (and other synthetic toxin analogs) on the gating properties of the Nav1.7 sodium channels was studied by Motin et al. (2016) using voltage clamp whole cell and single channel recordings in Chinese hamster ovary (CHO) cells expressing human Nav1.7 channels. They found that 322 the decay phase of the Nav1.7 channel opening slows down in a concentration-dependent manner 323 in the presence of these toxins. Using a paired-pulse protocol in the voltage clamp configuration, the 324 authors demonstrated an enhancement of Nav1.7 recovery from fast inactivation. Single channel 325 recordings showed that the mean open time of the channels was not substantially changed by the 326 toxin, but the channels exhibited a prolonged flickering behavior between open and closed states, 327 which enabled a more efficient inactivation removal. These experiments pointed to a voltage-sensor 328 trapping interpretation, in which the toxin prevents a conformational change in the domain IV 329 voltage sensor, as the main cause for the observed prolongation in the current duration. Motin et al. 330 (2016) also found that the current-voltage relationships of Nav1.7 are shifted to more negative 331 potentials in the presence of OD1, but this effect has a small magnitude (-3 mV), in accordance with 332 earlier observations in Xenopus laevis oocytes with Nav1.7 channels expression (Maertens et al., nanuscript 333 2006).

Our findings corroborate those of Motin et al. (2016). Indeed, we observed an increase in the 334 335 proportion of electrodes showing spontaneous firing in the presence of OD1, as well as an increase 336 in firing rate in cells that did fire before adding the toxin. In addition to the firing frequency rise, we 337 found a consistent increase in the spike amplitude after OD1, in contrast with the PF-05089771 338 treatment which affected only the firing rate. These larger extracellular spikes are in accordance 339 with the increase in peak current observed in the presence of OD1 in voltage clamp experiments 340 (Maertens et al., 2006; Motin et al., 2016). Since the amplitude of the current generated by the 341 opening of a single channel was not modified by OD1 (Motin et al., 2016), the size increase of the 342 extracellular spikes must be due to the dynamics of the gating process. In the next section, we 343 address the numerical simulations to offer an explanation for the changes in spike rate and 344 amplitude described above.

## 345 Numerical simulations

15

346 The computational model that we present here is able to provide satisfactory explanations at a 347 qualitative level for the main experimental findings of our study and for previous studies on 348 erythromelalgia and the effects of pharmacological manipulations on Nav1.7 channels. We did not 349 attempt to perform a complete exploration of the parameter space but all values are biologically 350 plausible. In the absence of stimulation the membrane potential tends to its fixed point which is the 351 resting potential. By injecting an amount of current also plausible for a patch clamp experiment 352 (0.037 nA for  $d_m = -58$  mV and  $g_{max} = 0.1$  S/cm<sup>2</sup>), the system reaches a Hopf bifurcation (e.g., 353 Ermentrout and Terman, 2010), the critical point corresponding to the spike threshold. At a critical 354 point, the stability of the system switches and a periodic solution of repetitive spiking arises, eliciting 355 pain. In the dark blue area of no firing of Fig 4 the membrane potential is at a fixed point (resting potential). The periodic solution occurs in the areas having other colors (including lighter tones of 356 blue). The Hopf bifurcation happens at the limit between the dark blue and the other colors, roughly 357 resembling a diagonal trajectory in the heat map. The descending transition from 1 to 2 and 4 358 359 exemplifies the trajectory towards pain in erythromelalgia and the horizontal transitions from 2 to 3 360 and from 4 to 5 and 6 depict the analgesic path triggered by PF-05089771.

361 While the decrease of Nav1.7 maximum conductance accounted for the analgesic effects of PF-362 05089771, OD1 effects on the firing rate were reproduced by enhancing the constant governing the 363 removal rate of the inactivation  $a_b$  (Fig 5). The interpretation of these results is quite straight 364 forward, having fewer available Nav1.7 receptors reduces the firing by interfering with the 365 amplification of subthreshold potentials performed by the channel, while the faster inactivation 366 removal increases the current size and duration (Fig 7), leading to increased spiking and excitability. 367 This is in line with the proved analgesic effects of Nav1.7 blockers (Cao et al., 2016) and with the 368 intense pain known to be experienced after a scorpion sting (e.g., Garfunkel et al., 2007).

In the case of spike amplitude, the explanation of the results requires a deeper elaboration. Starting
from the fact that spike depolarization is sustained by sodium currents, we can see that the

maximum amplitude that a spike can potentially reach in the absence of inactivation is given by the sodium equilibrium potential. The inactivation process will also limit the maximum value reached by the current and the peak intracellular voltage, because the current starts to inactivate before the opening process is completed. If this reasoning is correct, an increase of the inactivation removal rate of Nav1.7 will create a larger spike, because more channels will be free from inactivation during the critical period of the spike rising phase.

377 This last interpretation is exemplified in the numerical simulations of Figs 6 and 7. The consequences 378 of the faster inactivation removal rate of Nav1.7 after OD1 are noticeable in the higher values of the 379 process h, as well as in its faster return to 1 following the negative peak. The closer to 0 h reaches, 380 the more channels are inactivated, so a larger h value implies more open channels potentially 381 available, which is reflected in a larger Nav1.7 current (Fig 7-A). The high threshold Na<sup>+</sup> current also 382 grows slightly following enhancement of Nav1.7, without large changes of h. This increase is less 383 pronounced than for Nav1.7, but still contributes to increase the spike size because the total HH 384 type current is bigger. We must keep in mind that the extracellular spike is a filtered version of the 385 intracellular spike and we cannot necessarily compare the amplitude differences linearly. In addition, 386 Nav1.7 and Nav1.8 interact in a complex manner to regulate DRG neuronal excitability, as has been 387 shown in a previous modelling study of the rat HRV neurons (Choi and Waxman, 2011). Despite 388 these caveats, we can assume that in the situation depicted in our simulation both currents are 389 adding up to enhance the intracellular spike (Fig 6). This effect was captured in our extracellular 390 recordings (Fig 1).

391 Model limitations

We are interested in understanding the reason for the observed changes in spike rate and amplitude created by the two compounds tested using a model simulation with biologically plausible parameters. In this context, we validated our interpretation of biological facts with a numerical simulation. In order to keep the model simple and with a clear biological meaning and physical unit 396 for all variables, we opted for a modified HH scheme, which also has the virtue of being familiar to 397 neurobiologists. We included only one potassium current (non-inactivating, HH type), to avoid 398 unnecessary complexity. The only added current to the original HH scheme is the Nav1.7, because it 399 is strictly needed to implement the biological mechanisms under consideration. A detailed 400 quantitative modelling would require  $Ca^{2+}$  currents and several types of Na<sup>+</sup> and K<sup>+</sup> currents that have been found in mammalian DRG cells (e.g., Rush et al., 2007; Scroggs and Fox, 1992; Choi and 401 402 Waxman, 2011; Newberry et al., 2016; Mandge and Manchanda, 2018; Zemel et al., 2018), and is 403 beyond the scope of this study. Although more refined kinetic models of the Nav1.7 sodium and 404 other channels have been proposed (e.g., Sigg, 2014), we think that we are adopting here a level of simplification in the modelling process that is fitted for our purpose. 405 script DOI for

#### Extracellular recordings and ionic currents 406

Although extracellular recordings are typically used to detect firing times, they also have the 407 408 theoretical ability to report about what are considered to be intracellular features of the action 409 potential (Gold et al., 2006). We want to highlight this possibility of using extracellular recordings to 410 detect changes in ionic currents. If researchers first evaluate them together with voltage clamp data 411 for validation purposes, they can then benefit from the opportunity to observe more neurons 412 simultaneously. A small amplitude change of the DRG neuron spike might not play an important 413 physiological role in pain signalling, which is mainly conveyed by the spike rate, but we provided 414 here a proof of principle regarding the footprint of a current in the extracellular spike.

415 The fact that the extracellular spike did not show large changes in waveform shape with the 416 treatments (only scaling up moderately with OD1) facilitated our analysis, allowing reasonable 417 assumptions regarding neuron identities before and after the treatments, but this might not be the 418 case for other drugs or experimental systems (Hilgen, personal communication). It has been reported that an intracellular spike broadening caused by  $K^*$  current modulators can increase Ca<sup>++</sup> 419 420 influx at the synaptic level in mouse hippocampal cultures (Vivekananda et al., 2017). In this context it makes sense to speculate about the possibility that, if a larger spike could elicit more
neurotransmitter release, then the spike amplitude would also contribute to pain signalling by
eliciting a discharge of higher frequency in the ascending spinal neurons.

#### 424 Importance of the interaction between sodium currents

425 The interaction between sodium currents can have profound functional consequences, and the clinical signs of erythromelalgia provide a striking example (Rush et al., 2006). As explained above, in 426 427 pain pathways Nav1.7 increases neuronal excitability mainly by amplifying the depolarization caused 428 by peripheral stimuli, allowing to trigger Nav1.8. This facilitates firing and pain, an effect that is 429 exaggerated in erythromelalgia patients. A key property for this firing to occur (as implemented in 430 our model) is that Nav1.8 does not inactivate until the voltage is quite high (e.g., around -35 mV). In the sympathetic nervous system the situation is different because there are no Nav1.8 channels and 431 432 spikes are sustained by other sodium currents that inactivate at lower voltage (Rush et al., 2006). 433 Then, the excessive depolarization created by a mutated Nav1.7 in erythromelalgia can be sufficient 434 to trigger inactivation, terminating the firing. The excessively active mutated Nav1.7 increases firing 435 in HRV nociceptive neurons but blocks firing in the sympathetic nerves that mediate the contraction 436 of peripheral blood vessels. This results in excessive vasodilatation, creating the typical sign of red 437 extremities that originated part of the name to the disease (erythromelalgia could be translated as 438 "red neuralgia of the extremities"). The importance of the interaction between sodium currents is 439 highlighted by this example, because the same mutation produces opposite effects in the firing of 440 pain afferents and autonomic motor neurons.

#### 441 Figure captions

Fig 1. Effects of OD1 in nociceptive neurons. (A) Voltage data of the most active channel in MEA 1 before (upper panel) and after (lower panel) OD1 (100 nM) application. Note the increase in rate and amplitude of the spontaneous activity. (B) Rate and amplitude of paired neurons before and after OD1 (100 nM) application. Corresponding pairs in both plots are color coded. Wilcoxon signed 446 rank test p values are printed in each panel. The normalized changes of both indexes are highly 447

correlated (r = 0.78).

448 Fig 2. Effects of PF05089771 in nociceptive neurons. (A) Example of voltage data before and after 449 PF05089771 (100 nM).  $K^{+}$  concentration was 6 mM. (B) Rate and amplitude of the neurons paired 450 before and after treatment.  $K^{+}$  concentration was 4.16 mM. (C) Same as in B with a  $K^{+}$  concentration 451 of 6 mM. Wilcoxon signed rank test p values are printed in panels B and C, corresponding pairs are colour coded. The normalized changes in both indexes are poorly correlated (r = 0.21 in B and 0.53 in 452 453 C).

454 Fig 3. Erythromelalgia and PF05089771 effects: simulation of membrane voltage. Response of the model neuron to a 60 ms depolarizing pulse of 0.04 nA for three different values of half activation 455 456 voltage  $d_m$  (in mV) and maximum conductance  $g_{max}$  (in S/cm<sup>2</sup>). The numbers with circles in the panels 457 correspond to the numbers inside the white circles of Fig 4.

458 Fig 4. Erythromelalgia and PF05089771 effects: heat map of the spiking activity. The neuron model 459 spike rate is represented (color bar) for different values of maximum conductance  $g_{max}$  (abscissas) 460 and half activation voltage parameter  $d_m$  (ordinates) of the Nav1.7 current. The numbers in the 461 white circles correspond to the numbers in the panels of Fig 3. The dashed line on top indicates an 462 axis break.

463 Fig 5. Simulation of OD1 effects on the spike rate. Response to a 60 ms depolarizing pulse of 0.04 464 nA before (blue plots in left panels) and after (red plots in right panels) a 10 fold increase in the 465 inactivation removal rate  $a_h$  to simulate OD1 treatment. The value of  $d_m$  was varied from 57.8 mV 466 (upper panels) to 58 mV (lower panels), while  $A_h$  was varied from 0.92 (left panels) to 9.2 (right 467 panels).

468 Fig 6. Simulation of OD1 effects on the spike amplitude. Spikes with different removal rates of 469 Nav1.7 inactivation (parameter  $A_h$  = 0.92 in blue plot and 9.2 in red plot, with  $d_m$  = -58 mV). The red 470 spikes are slightly taller than the blue spikes (7 % average amplitude increase in a 5 s simulation).

20

Fig 7. Simulation of OD1 effects on Na<sup>+</sup> currents and their gating variables. Values of m (thin full lines), h (dashed lines) and Na<sup>+</sup> currents (thick full lines) during a spike. The currents were plotted in 10 x S/cm<sup>2</sup> and sign inverted for scale display purposes, as m and h always range from 0 to 1.  $A_h$  (in Nav1.7 only) was set to 0.92 in the blue plots (simulation before OD1) and to 9.2 in the red plots (simulation after OD1). (A) Nav1.7, note the higher h values after OD1. (B) High threshold Na<sup>+</sup> current, note that h is similar before and after OD1.

477 **References** 

478 Abdo H, Calvo-Enrique L, Martinez Lopez J, Song J, Zhang MD, Usoskin D, El Manira A, Adameyko I,

479 Hjerling-Leffler J, Ernfors P. Specialized cutaneous Schwann cells initiate pain sense. *Science* 365:
480 695-699, 2019.

Belzer V, Hanani M. Nitric oxide as a messenger between neurons and satellite glial cells in dorsal
root ganglia. *Glia* 67(7):1296-1307, 2019.

Blatt M, Wiseman S, Domany E. Superparamagnetic Clustering of Data. *Phys Rev Lett.* 76:3251-3254,
1996.

485 Cao L, McDonnell A, Nitzsche A, Alexandrou A, Saintot PP, Loucif AJC, Brown AR, Young G, Mis M,

486 Randall A, Waxman SG, Stanley P, Kirby S, Tarabar S, Gutteridge A, Butt R, McKernan RM, Whiting P,

487 Ali Z, Bilsland J and Stevens EB. Pharmacological reversal of a pain phenotype in iPSC-derived sensory

488 neurons and patients with inherited erythromelalgia. *Sci Transl Med* 8, 335ra56335ra56, 2016.

489 Carnevale T. Neuron simulation environment. *Scholarpedia* 2(6):1378, 2007.

490 Choi JS, Waxman SG. Physiological interactions between Nav1.7 and Nav1.8 sodium channels: a

491 computer simulation study. *J Neurophysiol*. 106: 3173-3184, 2011.

492 Dib-Hajj SD, Yang Y, Black JA, Waxman SG. The Na(V)1.7 sodium channel: from molecule to man. Nat

493 *Rev Neurosci.* 14 (1): 49-62, 2013.

21

- 494 Doi S, Nabetani S, Kumagai S. Complex nonlinear dynamics of the Hodgkin-Huxley equations induced
- 495 by time scale changes. Biol Cybern. 85 (1): 51-64, 2001.
- 496 Ermentrout GB, Terman DH. Mathematical Foundations of Neuroscience. New York: Springer, 2010.
- 497 Garfunkel LC, Kaczorowski JM, Christy C, editors. Pediatric Clinical Advisor. 2nd ed. Philadelphia:
- 498 Mosby, 2007.
- 499 Gold C, Henze DA, Koch C, Buzsáki G. On the Origin of the Extracellular Action Potential Waveform: A
- 500 Modeling Study. J Neurophysiol. 95 (5): 3113-3128, 2006.
- 501 Hilgen G, Sorbaro M, Pirmoradian S, Muthmann JO, Kepiro IE, Ullo S, Juarez Ramirez C, Puente
- 502 Encinas A, Maccione A, Berdondini L, Murino V, Sona D, Cella Zanacchi F, Sernagor E and Hennig MH.
- 503 Unsupervised Spike Sorting for Large-Scale, High-Density Multielectrode Arrays. Cell Reports manuscri
- 504 18(10): 2521-2532, 2017.
- 505 Khouzam RH. Chronic pain and its management in primary care. South Med J. 93(10):946-945, 2000.
- 506 Krouchev NI, Rattay F, Sawan M, Vinet A. From Squid to Mammals with the HH Model through the
- 507 Nav Channels' Half-Activation-Voltage Parameter. PLoS ONE 10(12): e0143570, 2015.
- 508 Lera Ruiz M, Kraus RL. Voltage-Gated Sodium Channels: Structure, Function, Pharmacology, and
- 509 Clinical Indications. J. Med. Chem. 58: 7093-7118, 2015.
- 510 Maeda E, Robinson HPC, Kawana A. The mechanisms of generation and propagation of synchronized
- 511 bursting in developing networks of cortical neurons. J Neurosci. 15 (10): 6834-6845, 1995.
- 512 Maertens C, Cuypers E, Amininasab M, Jalali A, Vatanpour H, Tytgat J. Potent modulation of the
- 513 voltage-gated sodium channel Nav1.7 by OD1, a toxin from the scorpion Odonthobuthus doriae. Mol
- 514 Pharmacol. 70 (1): 405-414, 2006.
- 515 Mandge D, Manchanda R. A biophysically detailed computational model of urinary bladder small
- 516 DRG neuron soma. PLoS Comput Biol. 14(7): e1006293, 2018.

- 517 McDonnell A, Schulman B, Ali Z, Dib-Hajj SD, Brock F, Cobain S, Mainka T, Vollert J, Tarabar S,
- 518 Waxman SG. Inherited erythromelalgia due to mutations in SCN9A: natural history, clinical
- 519 phenotype and somatosensory profile. Brain 139 (4): 1052-1065, 2016.
- 520 McDougal RA, Morse TM, Carnevale T, Marenco L, Wang R, Migliore M, Miller PL, Shepherd GM,
- 521 Hines ML. Twenty years of ModelDB and beyond: building essential modeling tools for the future of
- 522 neuroscience. J Comput Neurosci. 42(1):1-10, 2017.
- 523 Motin L, Durek T, Adams DJ. Modulation of human Nav1.7 channel gating by synthetic  $\alpha$ -scorpion
- 524 toxin OD1 and its analogs. Channels 10 (2): 139-147, 2016.
- 525 Newberry K, Wang S, Hoque N, Kiss L, Ahlijanian MK, Herrington J and Graef JD. Development of a
- 526 spontaneously active dorsal root ganglia assay using multiwell multielectrode arrays. J Neurophysiol.

#### 527 115(6): 3217-3228, 2016.

- anuscript Quian Quiroga R, Nadasdy Z, Ben-Shaul Y. Unsupervised Spike Detection and Sorting with Wavelets 528 529 and Superparamagnetic Clustering. Neural Comp. 16:1661-1687, 2004.
- 530 Rush AM, Cummins TR, Waxman SG. Multiple sodium channels and their roles in electrogenesis
- 531 within dorsal root ganglion neurons. J Physiol 579 (1): 1-14, 2007.
- 532 Rush AM, Dib-Hajj SD, Liu S, Cummins TR, Black JA, Waxman SG. A single sodium channel mutation
- 533 produces hyper or hypoexcitability in different types of neurons. PNAS 103 (21): 8245-8250, 2006.
- 534 Scroggs RS, Fox AP. Multiple Ca2+ currents elicited by action potential waveforms in acutely isolated
- 535 adult rat dorsal root ganglion neurons. J Neurosci. 12 (5) 1789-1801, 1992.
- 536 Serpell M. Anatomy, physiology and pharmacology of pain. Surgery Oxford 24(10): 350-353, 2006.
- 537 Sigg D. Modeling ion channels: Past, present, and future. J. Gen. Physiol. 144 (1): 7, 2014.
- 538 Van Hecke O, Torrance N, Smith BH. Chronic pain epidemiology and its clinical relevance. Br J
- 539 Anaesth. 111 (1): 13-18, 2013.

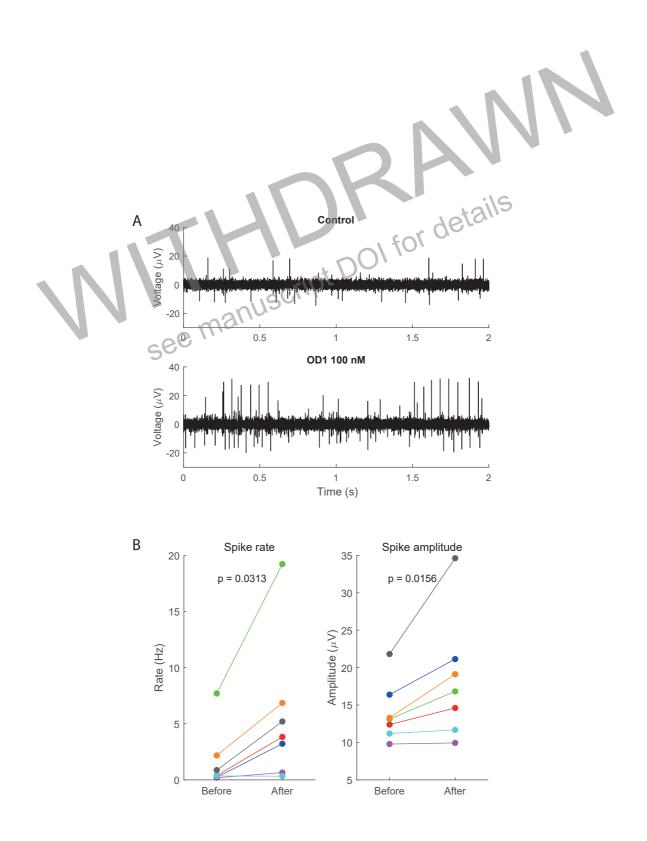
- 540 Vivekananda U, Novak P, Bello OD, Korchev YE, Krishnakumar DD, Volynski KE, Kullmann DM. Kv1.1
- 541 channelopathy abolishes presynaptic spike width modulation by subthreshold somatic
- 542 depolarization. *PNAS* 114 (9) 2395-2400, 2017.
- 543 Wilson PG, Stice SS. Development and differentiation of neural rosettes derived from human
- embryonic stem cells. *Stem Cell Reviews* 2(1): 67-77, 2006.
- 545 Zemel BM, Ritter DM, Covarrubias M, Muqeem T. A-Type KV Channels in Dorsal Root Ganglion
- 546 Neurons: Diversity, Function, and Dysfunction. Front Mol Neurosci. 11: 253, 2018.

# 547 Supporting information

- 548 **S1 Appendix. Equations Appendix.** Equations are from the HH model formulation provided by the
- 549 NEURON software and the Channel Builder GUI
- 550 (https://www.neuron.yale.edu/neuron/static/docs/chanlbild/main.html). Parameter values are
- 551 listed in Table 1 and provided with the corresponding figures.

# 552 Acknowledgements

553 Study funded by MRC BH171892.



bioRxiv preprint doi: https://doi.org/10.1101/871236; this version posted December 11, 2019. The copyright holder for this preprint (which was not certified by peer review) is the author/funder. All rights reserved. No reuse allowed without permission. -20 0 0.5 1 1.5 2 PF05089771 100 nM 20 Voltage ( $\mu$ V) 10 0 -10 -20 0 0.5 1 1.5 Time (s) В details Spike rate Spike amplitude 1.2 = 0.0313 = 0.4375 p 5 1 14 Amplitude 0.8 Rate (Hz) 0.6 12 0.4 10 0.2 0 8 Before Before After After С Spike rate Spike amplitude 15 30 p = 0.0005 p = 0.6791 25 Amplitude (µV) 05 10 Rate (Hz) 5 15 10 0 Before After Before After

